1972

The effect of internal pressure on axial fracture characteristics of internally surface-flawed specimens

Ralph N. Binkley
Lehigh University

THE EFFECT OF INTERNAL PRESSURE ON AXIAL FRACTURE CHARACTERISTICS OF INTERNALLY SURFACE-FLAWED SPECIMENS

by

Ralph N. Binkley

A Thesis

Presented to the Graduate Committee

of Lehigh University

in Candidacy for the Degree of

Master of Science

in

Metallurgy and Materials Science

Lehigh University

1972

CERTIFICATE OF APPROVAL

This thesis is accepted and approved in partial fulfillment of the requirements for the degree of Master of Science.

May 15, 1972
Date

John P. Wood
Professor in Charge

G. P. Cavard
Chairman of the Department
of Metallurgy and Materials
Science

ACKNOWLEDGEMENTS

The author wishes to thank Dr. J. D. Wood of the Lehigh University Metallurgy and Materials Science Department and Messrs. F. J. Fuchs and G. L. Schmehl of Western Electric Company, Inc., for their generous cooperation and useful suggestions throughout the course of this investigation. Further thanks are due many other individuals who provided equipment and help when possible.

TABLE OF CONTENTS

LIST OF FIGURES

LIST OF TABLES

ABSTRACT

Internally precracked thick-walled cylinders were fractured under uniaxial stress conditions both without and with internal pressure to determine the difference in fracture characteristics. The surface flaws were on the inside diameter and oriented so that a Mode I type opening occurred when a steadily increasing axial tension load was applied to the cylinder. The triaxial stress state at the crack tip was modified by internally pressurizing to 60,000 psi.

A modified air-melted H-11 alloy steel known as Vascojet 1000, heat treated to yield strength of 203,000 psi. was tested with wall thicknesses of 0.125 and 0.150 inches. Surface flaw depths were from 0.012 inch deep to approximately the middle of the wall thickness in each specimen size.

Internal pressure increased the axial net fracture stress for fractures under stress state conditions which were mixed plane-strain plane-stress states. The application of flat-plate surface flaw analysis based on fracture mechanics gave unrealistically low estimates of the stress intensity. Percent shear lip is not changed by internal pressure within a cylinder. An empirical equation was proposed to estimate the fracture of pressurized cylinders based on the Von Mises fracture stress. Subcritical flaw growth appears to have occurred in the pressurized cylinders primarily in the flaw width direction. The complex loading and interaction with the pressurizing media are possible factors to explain the subcritical crack growth.

I. INTRODUCTION

A. General

Fracture failures of pressurized cylinders often originate from surface flaws on the interior surfaces. One method of predicting fracture behavior[1-3] under uniaxial loading conditions is the stress intensity concept by using linear elastic analysis or by using plasticity models. The main difficulty in applying these concepts occur in computing the value of the stress intensity factor for a given method of loading, crack configuration and specimen geometry. Although stress intensity factors for various combinations[4,5] are available, the stress intensity factors for surface flaw configurations in curved surfaces would be very complex[6] and are not presently available. Sih and Setzer[7] have shown that the crack tip stress fields are equivalent to combining modes I and II with a bending field. Modes I and II result from the extension of the middle surface of the cylinder, and the bending fields result from changes in the curvature of the middle surface when necking occurs. They also observed that the extension and bending effects would result in stress intensity factors involving many parameters.

The introduction of biaxial or triaxial loading conditions at the crack tip present further complications[8] in applying present stress intensity concepts. Some work has been done with biaxial loading by Kibler and Roberts[9] on center cracked plates. They have shown that for biaxial loading conditions, the existing

linear elastic analyses and plasticity models[10] do not account for the strengthening effect produced by the biaxial loading for plane stress fractures. Although surface flaws and triaxial loading conditions normally occur in actual applications of pressurized cylinders, little work has been done relating the fracture characteristics to the complex loading conditions.

B. Surface Flaw Analysis

Since the surface flaw analyses are not available for curved surfaces, the surface flaw analyses for flat plates was used as an approximation. The plane-strain stress intensity factor K_I as proposed by ASTM[11] for semielliptical surface flaws in flat-plate test specimens under remote axial Mode I loading is

$$K_I = 1.1\sqrt{\pi}\,\sigma\left(\frac{a}{Q}\right)^{1/2} \qquad (1)$$

where σ is the gross applied stress, a is the flaw depth or the semiminor axis of the elliptical flaw contour and Q is a parameter that is a function of flaw shape, σ and the 0.2% offset yield strength. Equation 1 was first proposed by Irwin[12,13] and was based on the elasticity solution derived by Green and Sneddon[14]. The parameter Q is defined as

$$Q = \Phi^2 - 0.212\left(\frac{\sigma}{\sigma_{YS}}\right)^2 \qquad (2)$$

where σ_{YS} is the 0.2% offset yield strength and Φ is the complete elliptical integral of the second kind corresponding to

$$\Phi = \int_0^{\pi/2} \left[1 - \left(\frac{c^2 - a^2}{c^2} \right) \sin^2 \theta \right]^{1/2} d\theta \qquad (3)$$

where c is the semimajor axis of the elliptical flaw contour and θ is the angular displacement from the semiminor axis. The maximum value of K_I occurs at the end of the semiminor axis of the ellipse and at flaw instability, Equation 1 can be written

$$K_c = 1.1\sqrt{\pi}\, \sigma \left(\frac{a_c}{Q} \right)^{1/2} \qquad (4)$$

where the subscript letter c indicates crack instability conditions. A crack area limit of 10 percent of the gross area and the specimen size requirements shown in Figure 1 were proposed by ASTM for the use of Equation 1.

Theoretically, elliptical flaws with identical a/Q values will have identical K_c and the a/Q value of a flaw provides a single parameter with which to correlate fracture data obtained from surface-flawed specimens with different flaw shapes. The ability of the parameter Q to characterize the severity of surface flaws in flat specimens has been investigated by several authors[15,16] with the general conclusion that the Q parameter adequately accounted for the severity of the surface flaw with respect to the

crack shapes and to plane-strain stress intensity calculations.

Two proposed modifications to Equation 4 were considered in the specimen analysis. Paris and Sih[4] recommend that the front-face free-surface correction factor in Equation 4 should be a function of the a/c ratio given by

$$\left[1 - 0.12 \, (1 - a/c) \right] \tag{5}$$

instead of a constant value of 1.1. Randall[15] proposed that the K values should be multiplied by the correction factor;

$$\left[\frac{\text{gross area}}{\text{net area}} \right] \tag{6}$$

since the effect of the crack surface area is not accounted for by Irwin in Equation 1. These correction factors were not applied to Equation 4 since the influence of these factors was small for the a/c and area ratios used in this work.

C. Objectives

The objectives of this work were to study internally surface-flawed cylinders in the following ways:

1. Net fracture stress, with and without internal pressure.
2. Attempt to apply flat-plate surface flaw equations to cylindrical specimens without internal pressure.
3. Alteration of fracture appearance with internal pressure.

4. Engineering predictions of fracture stress with internal pressure based on the Von Mises fracture stress.

II. EXPERIMENTAL PROCEDURE

A. Preparation of Specimen

The specimens were machined from one inch diameter bars of air melted Vascojet 1000 alloy steel. The AISI designation of H-11 is normally used in literature for this martensitic steel. All bars were from the same heat and had a nominal composition of 0.40% C, 5.00% Cr, 1.30% Mo and 0.50% V. Figure 2 shows the specimen geometry and all specimens were machined the same with the exception that two outside diameters were used: 0.750 and 0.800 inches.

The specimens were rough machined prior to heat treating with extra material left on the inside diameter, outside diameter and on both threads. The heat treating was done in two separate groups in the following sequence:

1. Preheated to 1450°F in a protective atmosphere (dry argon).
2. Austenitize at 1850°F in the same atmosphere as above (automatic temperature controls, range of 1840 - 1860°F), for 30-35 minutes.
3. Air cool to 100-150°F.
4. Temper at 1100°F in air atmosphere (automatic temperature controls, range of 1090-1100°F) for 2.5 hours.
5. Air cool to below 200°F.
6. Temper at 1100°F in air atmosphere (same as step 4).
7. Air cool to room temperature.

After heat treating, the inside diameters were honed, the outside diameters ground and the threads were ground. The fatigue crack starter slot shown in Figure 3 was produced by the electric discharge machining (EDM) process using a 0.002 inch thick tantalum foil electrode. The EDM slots were 0.003 inches wide, 0.007 inches deep at the leading edge and had a 0.0015 inch tip radius. Very little structural damage was introduced by the EDM process as evidenced by photomicrographs.

Next the specimens were fatigued to initiate and grow a sharp crack by applying a varying axial tensile load at 10 cycles per second. For the final portion of the fatigue precracking, all specimens were fatigued with a maximum load corresponding to 40,000 psi gross stress (maximum estimated K value of 19,000 psi $\sqrt{\text{in.}}$) and a minimum load based on 2,000 psi gross stress. Specimens that have a plus sign in front of the number-of-cycles figure in Tables 1 or 2 were fatigued at a higher stress level for less or equal to 500 cycles to initiate the crack. Although the ASTM[17] fatigue crack requirements were not designed for surface flawed specimens, these stress values, maximum estimated K value and range are in general accord with the ASTM recommendations.

B. Axial and Internal Pressure Equipment

A schematic of the test equipment is shown in Figure 4 where the numbers used below in parenthesis refer to the schematic drawing. Tensile loads were applied to the test specimen by a six inch diameter hydraulic cylinder (1). The hydraulic pump

supplying the six inch cylinder was capable of supplying up to 3500 psi oil pressure. The applied load was measured with a Strainsert 100,000 pound capacity load cell (2) and the load measurements were recorded on a Brush 4-channel strip chart recorder (3).

The pressurized specimens were internally pressurized as closed end pressure chambers. The oil used was Mobil DT-E24 hydraulic oil and no attempt was made to remove the moisture content. The internal pressures for the test specimens were obtained by supplying hydraulic pressure from a second hydraulic pump to the 35,000 psi capacity intensifier (4). The output pressure from the first intensifier was increased by a factor of four by a 100,000 psi capacity intensifier (5). The output pressure from the 100,000 psi intensifier entered the test specimen through a manifold and a Norwood 100,000 psi capacity pressure transducer (6) recorded the hydraulic pressure on the same recorder that registered the load cell measurements. Special beryllium copper seals were used approximately one half inch from each end of the specimen on the inside diameter to hold the desired pressure levels inside the specimens.

The hydraulic pump unit supplying the six inch cylinder was set at 3,300 psi pressure and the flow rate was adjusted to give the specimen an average loading rate of approximately 600 pounds per second, which corresponds to strain rates of 0.00$5 and 0.00$4 inch/inch/minute in the 0.750 and 0.800 inch diameter specimens

respectively. Since the strain-rate sensitivity is small for martensitic steels heat treated to yield strengths in excess of 200,000 psi[3], the strain rates used will not adversely influence the data and are equal to or less than the conventional static fracture test strain rate of 0.005 inch/inch/minute. The pump capacity was sufficient to hold the 3,300 psi pressure constant while building up pressure in the six inch cylinder. The hydraulic pump unit supplying the 35,000 psi intensifier had a capacity of 3,000 psi pressure with variable flow rates and pressure. For the internally pressurized experiments the total time under internal oil pressure for each specimen was less than five minutes.

C. Measurements

Prior to the experiments the inside and outside diameters were measured with micrometers and recorded. Hardness values were recorded by taking the average of three readings on each end of the test specimen. Fatigue data recorded for each specimen consisted of the number of cycles, maximum applied force and the minimum applied force. During the experiment the axially applied force and the internal specimen pressure was recorded on the recorder at a speed of five millimeters per second.

Fractographic resolution of the fractured surfaces was good with properly oriented light and photographs were used at a known magnification to determine the chord angle of the critical flaw. A toolmaker's microscope combining optical magnification with micrometer table movement was used to measure the EDM notch depth,

critical flaw depth, width of flat fracture surface and width of the shear lip at the leading edge of the critical flaw. Most of the measurements taken were repeatable but two types of measurements involved human judgement. The major chord length of the critical flaw was determined by a projected elliptical contour based on the center portion of the flaw. Also, some of the critical flaw depths were not well defined and several measurements were averaged in these cases.

D. Specimen Analysis

1. General

K_{Ic} data has been reported[18] for the H-11 alloy steel tempered at 1100°F and were determined[19] to be valid plane strain K_{Ic} values. The average of eight notch-bend three-point-loaded tests using one inch square specimens was 73.2 ksi $\sqrt{\text{in.}}$ with the lowest value of 61.6 and the highest value of 80.1. The flaws in the above test specimens were tangentially oriented to the rolling direction and the flaws in the test specimens used in this work were similarly oriented. However, the tempering times for the valid K_{Ic} values were two hours plus two hours as compared to 2.5 hours plus 2.5 hours for the specimens used in this work. Hardness measurements were used to estimate yield strength from previously determined relationships[21] as shown in Figure 5. An approximation that is generally accepted[20] for a valid K_{Ic} value is that the crack depth and the ligament depth should both be $\geq 2.5 (K_{Ic} / \sigma_{YS})^2$ for through-cracked specimens. Based on the reported K_{Ic} value and

the above criteria, as an approximation, the minimum wall thickness necessary for valid K_{Ic} values in these specimens is 0.34 inches while the thickest wall used in these experiments was 0.15 inches. It is predicted that the specimens used in these experiments will have fractures exhibiting mixed plane-strain plane-stress modes.

The fracture mode transition[22] was based on the percentage of shear at the leading edge of the critical flaw as shown in Figure 6 and was calculated from

$$\% \text{ shear} = \frac{S}{S + Y} (100) \qquad (7)$$

where the shear lip depth S and the rapid flat fracture depth Y are both measured in the flaw specimen semiminor axis direction of the ellipse.

2. Unpressurized Specimens

The net axial critical stress σ_N was calculated by

$$\sigma_N = \frac{F}{0.785(D^2 - d^2) - 1.571\ a\ c} \qquad (8)$$

where F is the axial load, D is the outside diameter of the specimen, d is the inside diameter of the specimen, a is the flaw depth and c is one-half of the flaw width. The critical flaw contour was based on an elliptical contour approximating the middle third of the actual flaw contour. The flaw depth (a) was measured as shown in Figure 7 and the flaw width (2c) was the arc length on the inside

specimen diameter of the projected elliptical contour. The gross axial fracture stress was calculated by

$$\sigma_G = \frac{F}{0.785(D^2 - d^2)} \tag{9}$$

K values were calculated by applying Equation 4 to the curved surface specimens using the values of a and 2c as defined above. These values are called K_{exp} and are only approximate values instead of strictly correct K_c values.

3. Pressurized Specimens

The net axial critical stress σ_N was calculated by

$$\sigma_N = \frac{F + P}{0.785(D^2 - d^2) - 1.571\ (a)(c)} \tag{10}$$

where F is the externally applied axial force recorded by the load cell and P is the axial tension force on the specimen side walls resulting from the internal pressure acting of the ends of the interior chamber. Strain gages were used on some of the outside diameters to prove that the axial force resulting from the internal pressure would not be measured by the load cell.

Strain gage data from the unpressurized and pressurized specimens are shown in Figure 7. The strain gage data for the unpressurized specimen was used to calculate a Poisson ratio of 0.31 and modulus of elasticity of 28×10^6 psi for the material. The gross axial stress in the pressurized specimen was then calculated

from the strain gage data for the pressurized specimen and is compared in Figure 8 with the gross axial stress calculated from Equation 9. The gross axial stress calculated from the strain gages approximates the stress calculated from Equation 9 illustrating the validity of Equation 10.

The Von Mises fracture criterion σ_V relates the three principle stresses[23] existing in a triaxial stress state by

$$\sigma_V = \frac{1}{\sqrt{2}} \left[(\sigma_r - \sigma_t)^2 + (\sigma_t - \sigma_a)^2 + (\sigma_a - \sigma_r)^2 \right]^{1/2} \quad (11)$$

The relationship of σ_V to K_c and other parameters of the pressurized specimens were investigated in an attempt to predict fracture stress values for pressurized cylinders when the gross axial fracture stresses are known for the unpressurized cylinder. Stresses were calculated at the depth corresponding to the leading edge of the critical surface flaw[24]. The radial stress, σ_r, was calculated from

$$\sigma_r = \frac{p\,(r_i)^2}{(r_o)^2 - (r_i)^2} \left(1 - \frac{(r_o)^2}{b^2} \right) \quad (12)$$

where p is the internal pressure, r_i is the inside radius of the cylinder, r_o is the outside cylinder radius and b is the radius corresponding to the leading edge of the critical crack. The tangential stress, σ_t, was calculated from

$$\sigma_t = \frac{p\,(r_i)^2}{(r_o)^2 - (r_i)^2}\left(1 + \frac{(r_o)^2}{b^2}\right) \qquad (13)$$

The axial stress, σ_a, was assumed to be constant over the gross section area and equal to the sum of the stress due to the internal pressure p acting on the end of the internal chamber and the stress due to the externally applied force F using the relationship;

$$\sigma_a = \frac{p\,(r_i)^2}{(r_o)^2 - (r_i)^2} + \frac{F}{\pi(r_o^2 - r_i^2)} \qquad (14)$$

III. RESULTS AND DISCUSSION

The experimental test results for the 0.750 and 0.800 inch diameter specimens are shown in Tables 1 and 2, respectively. The calculations of K_{exp}, axial gross stress, axial net stress, yield strength, a/2c, Φ^2, a_c/Q, percent shear and Von Mises fracture stress for the unpressurized and pressurized specimens are shown in Tables 3 and 4, respectively.

A. Net Stress Relationship

The net-section axial fracture stress versus crack depth to wall thickness ratio, a_c/t, is given in Figure 9. Figure 10 was plotted versus $(a_c/Q)/t$ to show the influence of the shape parameter Q. Both figures have the same general form with the Q parameter giving a more gradual rise for the pressurized data with the deeper flaws and giving relatively larger $(a_c/Q)/t$ values for the pressurized data than for the unpressurized data. The Q parameter appears to better represent the severity of the crack and is used in this investigation.

The pressurized specimens exhibited higher axial net-section fracture stresses than the unpressurized specimens. This difference in fracture stress between the unpressurized and pressurized specimens increased as the critical flaw depths increased. As the critical flaw depths increased, the unpressurized specimens showed slightly decreasing fracture stresses and the pressurized specimens showed noticable increases in fracture stresses.

B. Unpressurized Specimen K Values

The stress intensity parameter was calculated from Equation 4 and was called K_{exp} due to the application to the curve surfaced specimens. In Figure 11, K_{exp} is plotted versus percent shear. Using the percent shear as the basis for plane-strain plane-stress fracture mode transition, all of the specimens exhibited mixed mode fractures. The thickest specimen wall was not thick enough as previously predicted to produce fractures with very small percentages of shear or result in values that could be interpreted as K_{Ic} values.

Figure 12 shows the change in K_{exp} as the $(a_c/Q)/t$ flaw dimension increases. Assuming that the crack tip stress state approaches plane-strain conditions as the crack gets shallower or the percentage shear lip decreases, the value of K_{exp}, an estimate of K_{Ic}, is considerably less than 62 ksi$\sqrt{in.}$ Based on the previously reported K_{Ic} value[18], K values from Equation 4 appear to be too low and cannot be used to predict valid critical stress intensity values in the unpressurized cylinders. Consequently, no attempt was made to use these equations for the pressurized states.

C. Shear Lip Trend

The percent shear is plotted versus $(a_c/Q)/t$ in Figure 13. The shear lip sizes for $(a_c/Q)/t$ values up to 0.50 were not influenced by the internal pressure. Both specimen sizes with and without internal pressure showed a linear relationship for $(a_c/Q)/t$ values up to 0.40.

Figures 14 and 15 illustrate the effect of crack depth on shear lips for cylinders with and without internal pressure. The arrows denote the critical cracks. The fracture surfaces had the smallest shear lip on the outside diameter of the specimen directly opposite the deepest portion of the critical flaw. Away from the critical flaw region, the shear lips on the outside diameter increased in size and were larger than the shear lips on the inside diameter.

D. Von Mises' Criterion

As an engineering approximation the Von Mises fracture stress defined by Equation 11 was compared for both pressurized and unpressurized specimens. Equation 11 when applied to unpressurized cylinders is the same as the axial gross-section fracture stress, σ_G. In Figure 16, the Von Mises fracture stresses are plotted versus $(a_c/Q)/t$. It is proposed that a relationship occurs between the pressurized and unpressurized specimens that appears to represent a constant displacement which can be described by

$$\sigma_V = \sigma_G + 23 \text{ ksi} \qquad (15)$$

This relationship is empirically based and no way has been found for theoretically calculating this displacement of the pressurized data line shown in Figure 16 from the unpressurized data line. Further work needs to be done using different internal pressures to determine if a more universal relationship can be derived.

E. Other Trends

The critical flaw contours differed between the unpressurized and pressurized specimens as shown in Figures 17 and 18. The arrows show the 2c dimensions for the projected elliptical contours. The pressurized specimens had wider critical flaws for similar flaw depths. The flaw depths were slightly deeper in general for the pressurized specimens even though the unpressurized specimens averaged similar or more fatigue cycles. It appears that subcritical flaw growth[25] occurred in the pressurized specimens either during the time under internal pressure and/or during the axial loading. Subcritical flaw growth could have possibly be introduced by the hydraulic oil (stress corrosion cracking) even though the maximum total time in contact with the oil was five minutes and the maximum time under the applied axial force was less than two minutes.

Subcritical flaw growth could also have been caused by the complex loading that existed at the crack front. The stresses caused by internal pressure superimposed on the applied axial stress result in a complex stress situation and therefore, the stress intensity at the crack front cannot be definitively described. In addition, the pressurizing media acts also on the surfaces of the flaw producing forces that further complicate the situation. Hartranft and Sih[26] have proposed that these forces acting alone will change the stress intensity profile in a way that would produce wider flaws.

IV. CONCLUSIONS

Internal pressure increased the axial net fracture stress for internally precracked cylinders fractured under mixed mode stress state conditions. The application of flat-plate surface flaw analysis based on fracture mechanics to the curved surface gave unrealistically low estimates of stress intensity.

Percent shear lip was not changed by internal pressure within a cylinder. An empirical equation was proposed to estimate the fracture stress of pressurized cylinders based on the Von Mises fracture stress.

Subcritical flaw growth appears to have occurred in the pressurized cylinders primarily in the flaw width direction. Interaction with the pressurizing media and the complex loading are possible causes of the subcritical flaw growth.

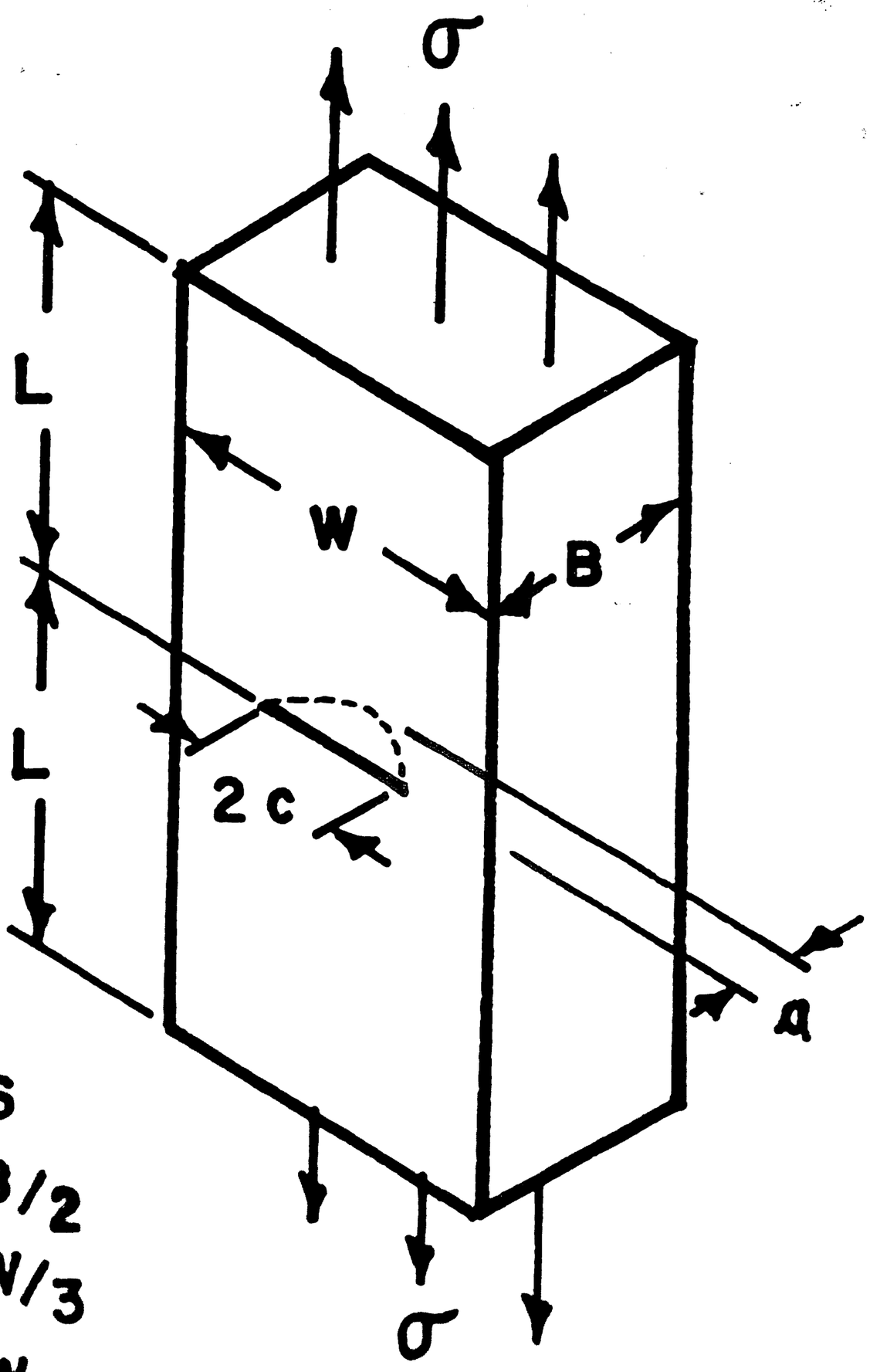

(1) $W/B \geq 6$

(2) $a < B/2$

(3) $2c \leq W/3$

(4) $L \geq W$

FIG. 1 — ASTM SURFACE FLAW REQUIREMENTS.[11]

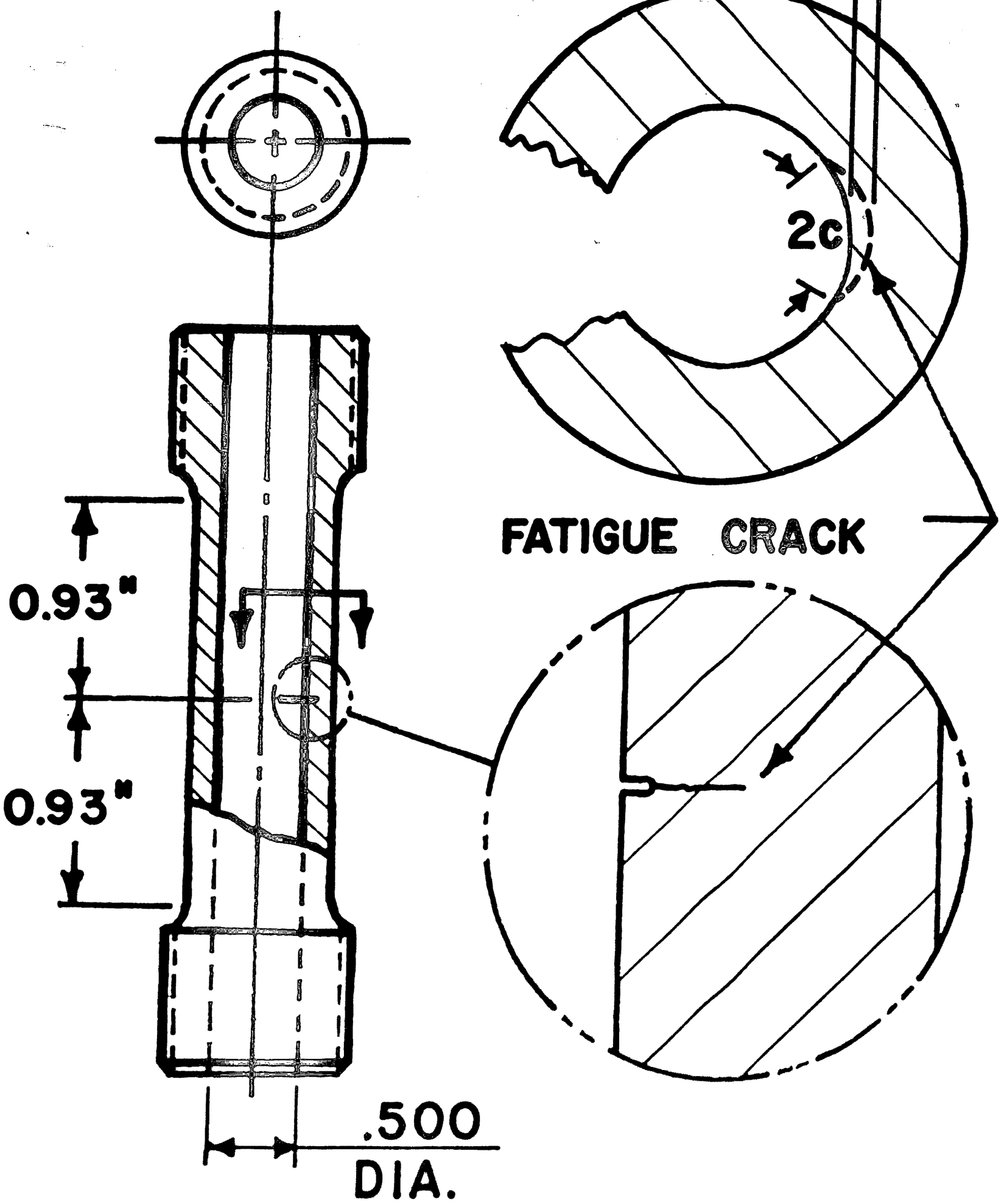

FIG. 2 – TEST SPECIMEN.

1000 X
(2% NITAL)

FIG. 3 — EDM FATIGUE-
CRACK STARTER NOTCH.

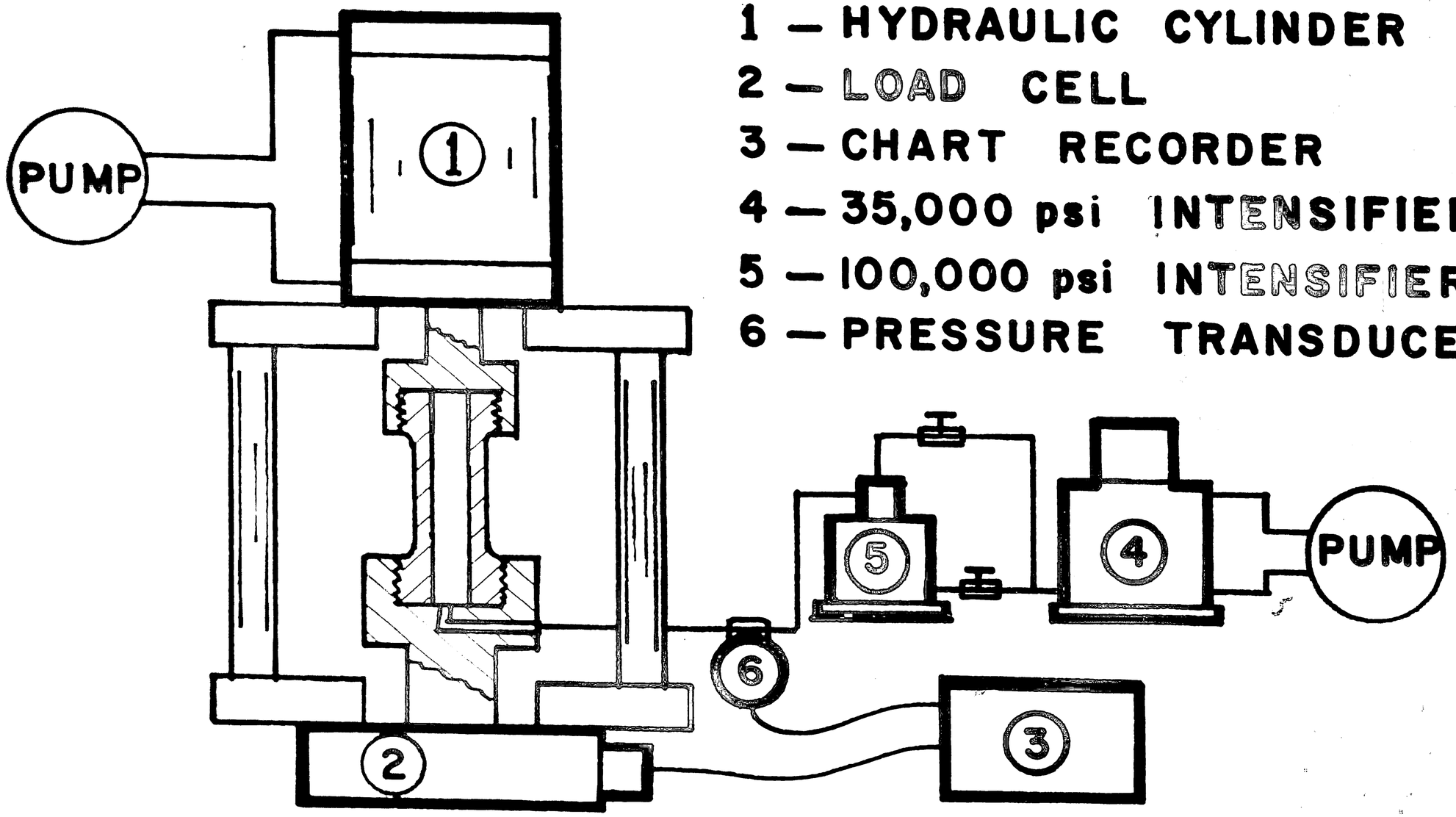

1 — HYDRAULIC CYLINDER
2 — LOAD CELL
3 — CHART RECORDER
4 — 35,000 psi INTENSIFIER
5 — 100,000 psi INTENSIFIER
6 — PRESSURE TRANSDUCER

FIG. 4 - SCHEMATIC DRAWING OF TEST EQUIPMENT.

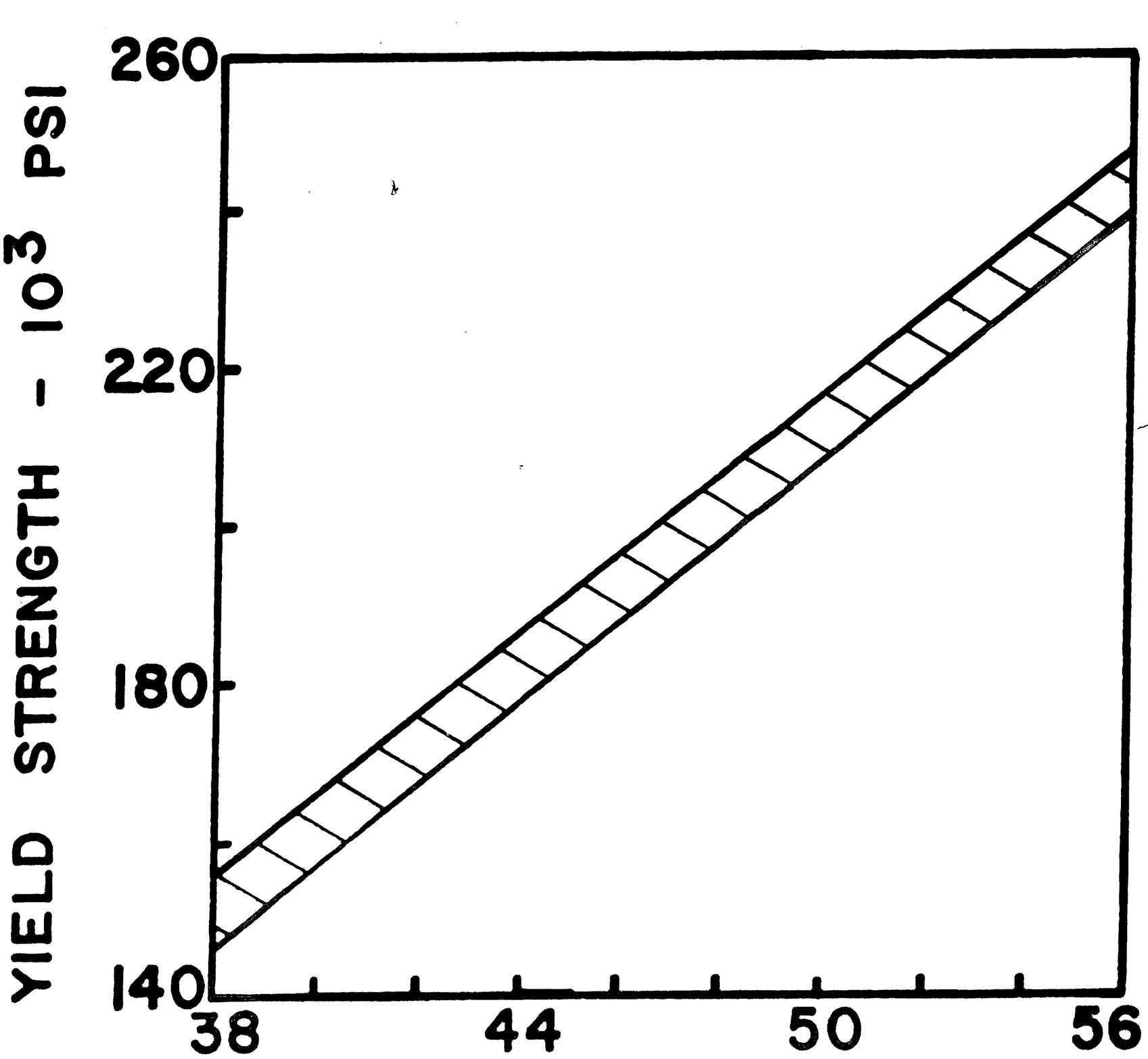

FIG. 5 - STRENGTH VS. HARDNESS FOR VASCOJET 1000.[21]

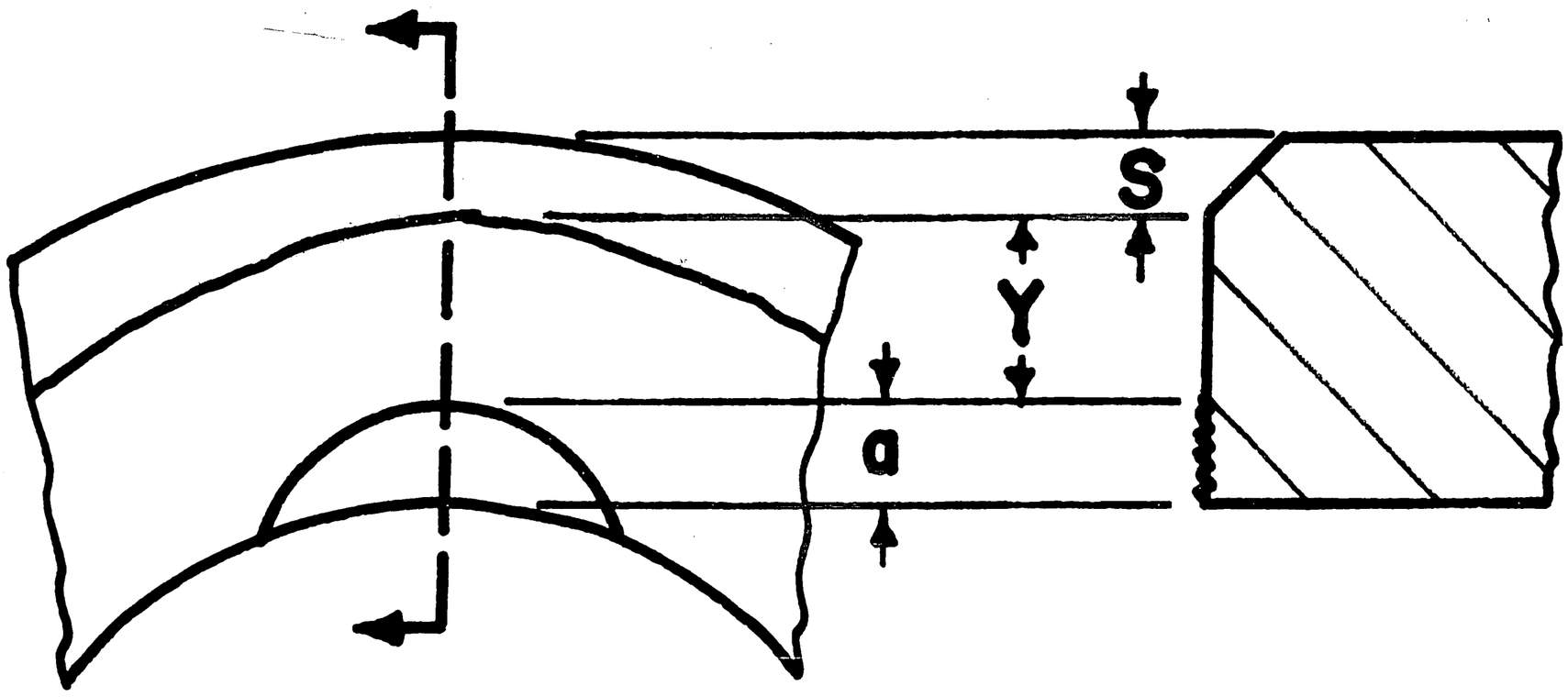

$$\% \ \text{SHEAR} = \frac{S}{S+Y}(100)$$

FIG. 6 - DEFINITION OF % SHEAR.

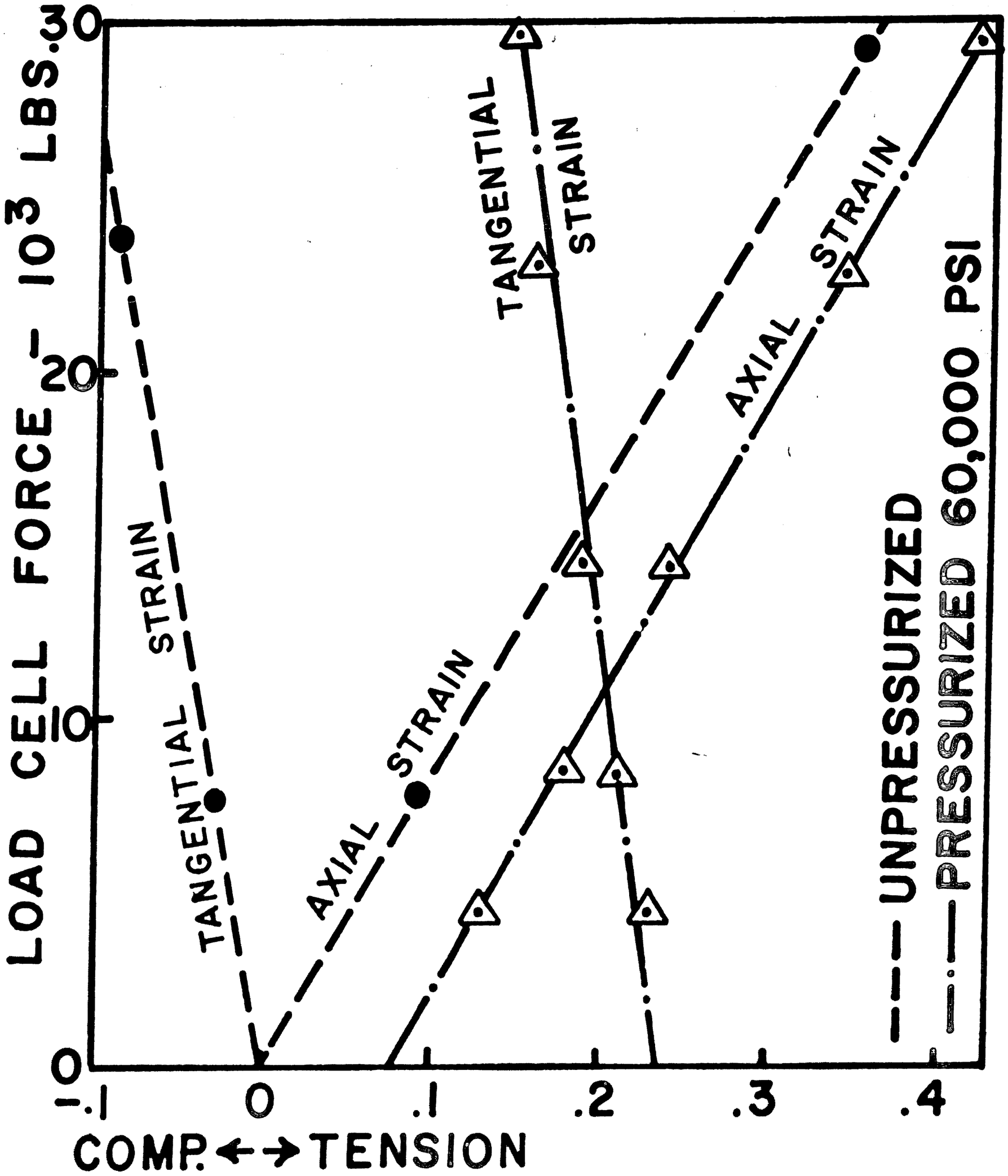

FIG. 7 — FORCE VS. STRAIN ON OUTSIDE DIA. OF .800 DIA. SPECIMENS.

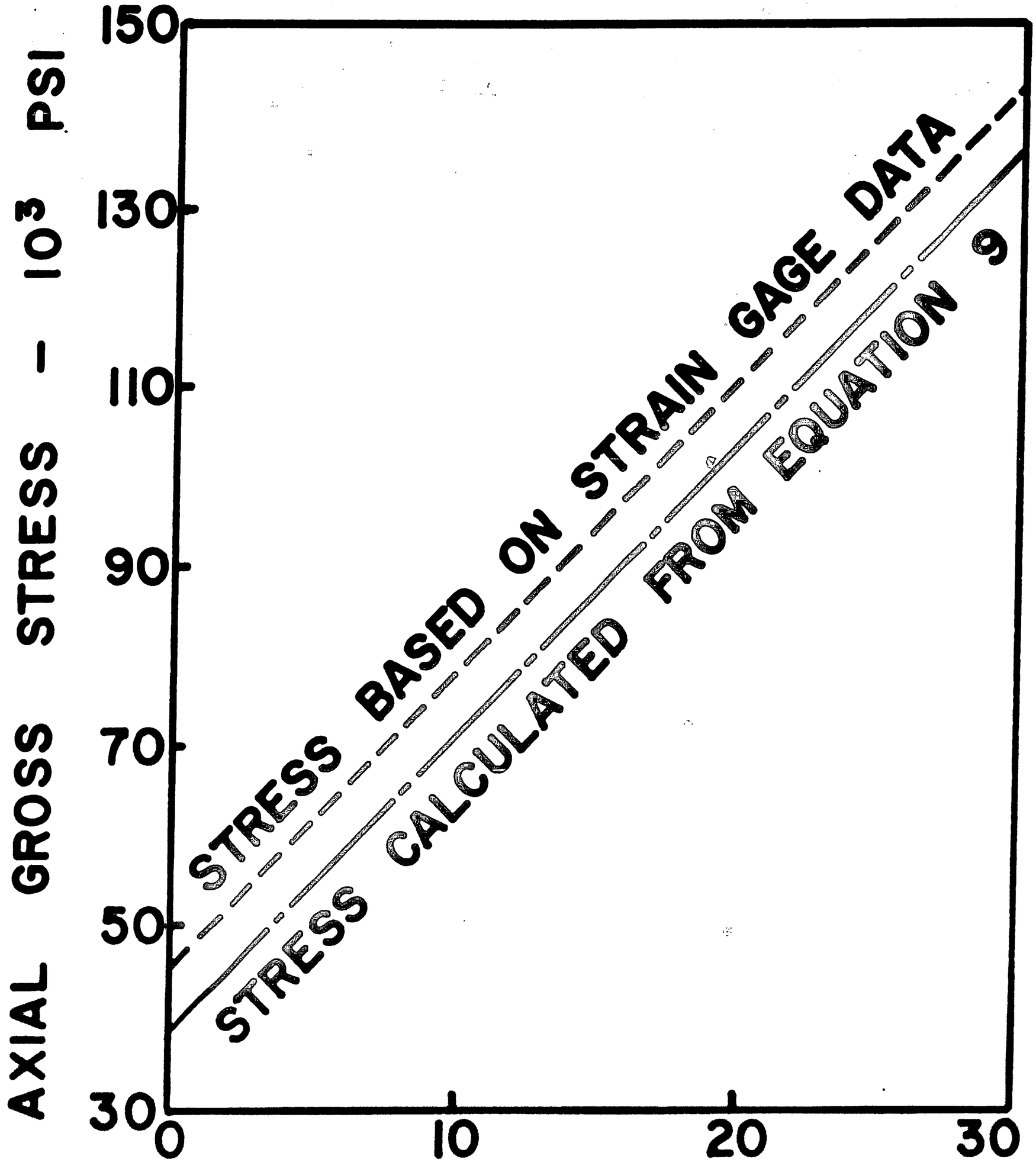

FIG. 8 - AXIAL GROSS STRESS VS. LOAD CELL FORCE ON .800 IN. DIA. SPECIMENS.

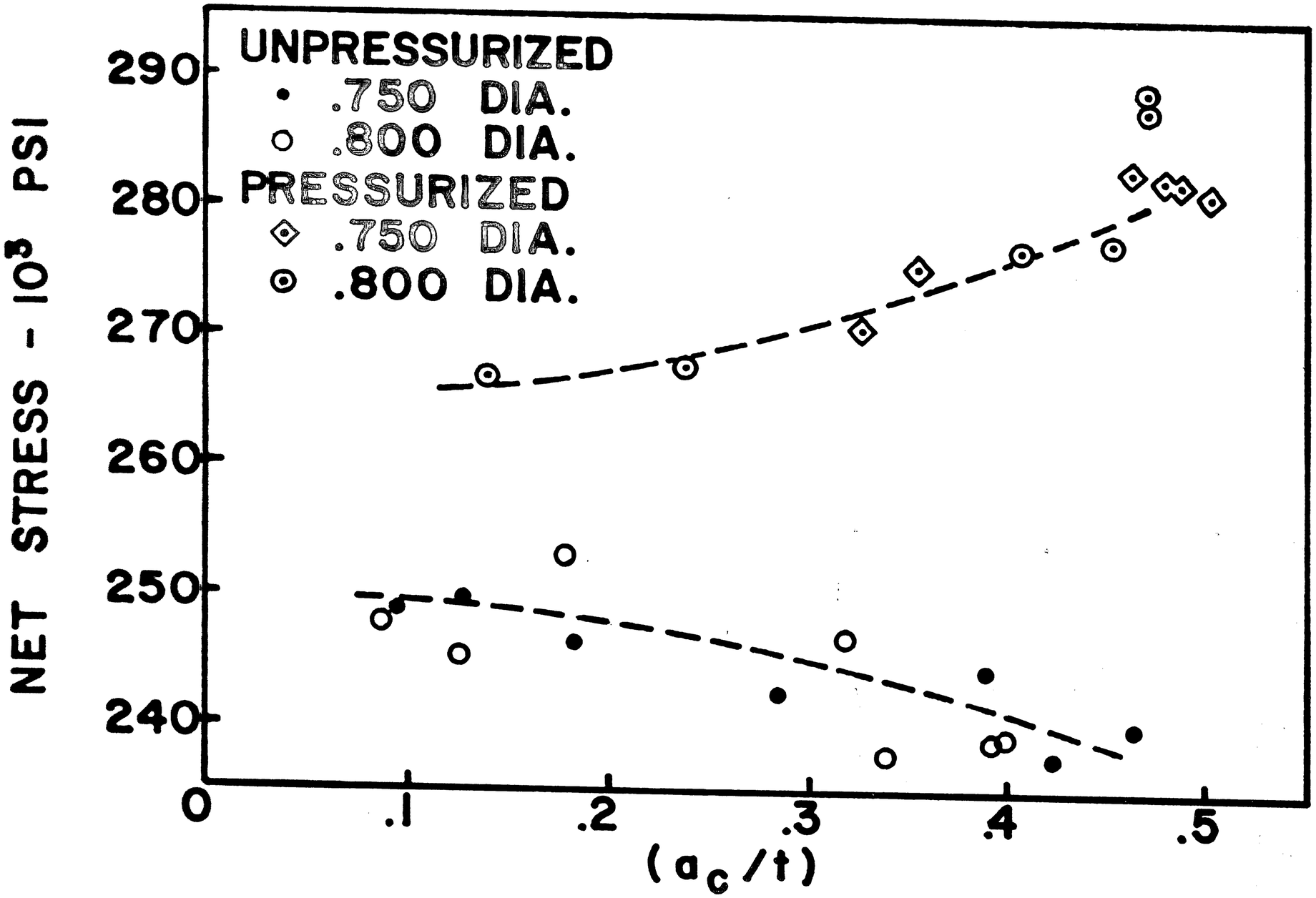

FIG. 9 – NET AXIAL FRACTURE STRESS VS. (a_c/t).

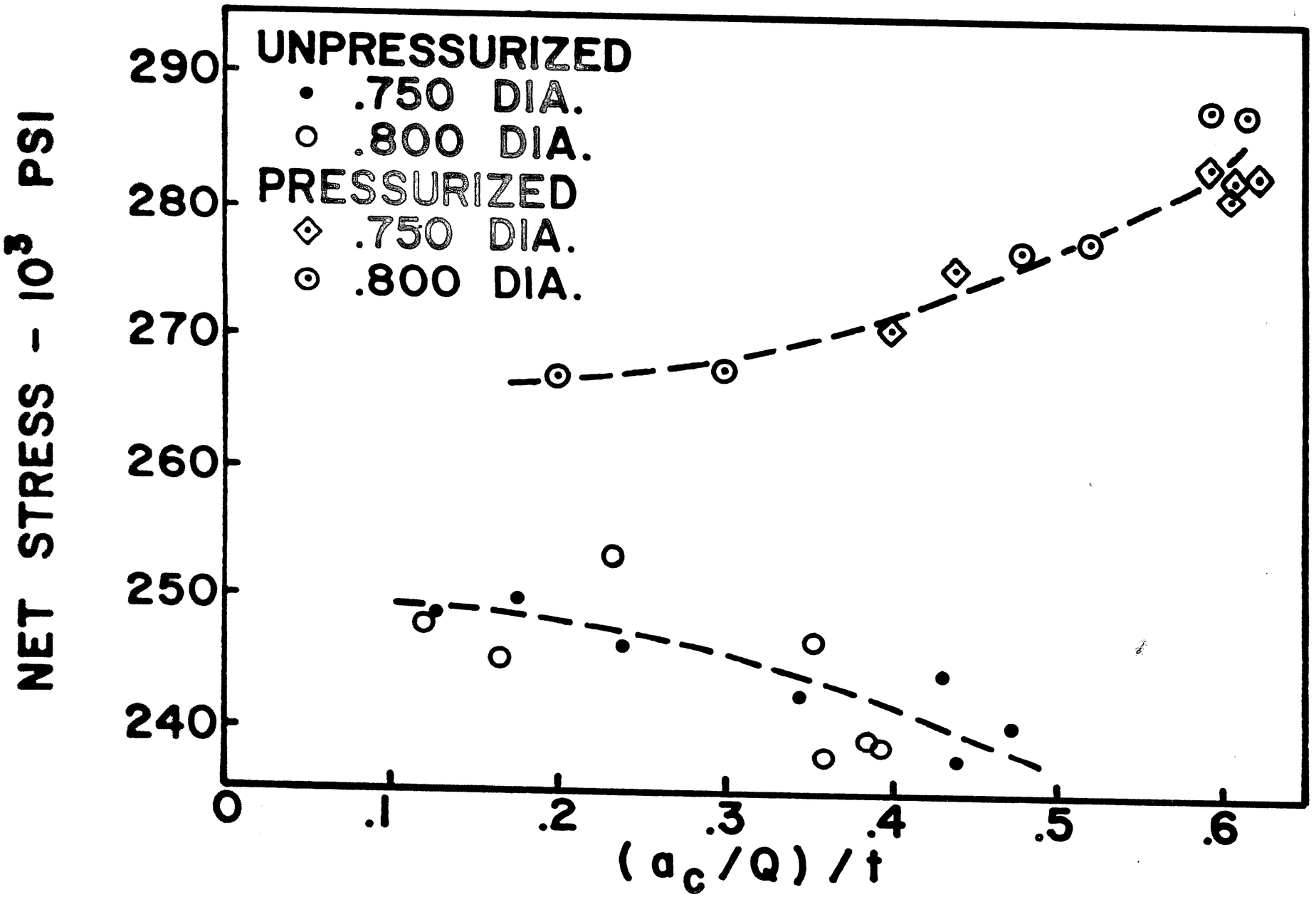

FIG. 10 - NET AXIAL FRACTURE STRESS VS. $(a_c/Q)/t$.

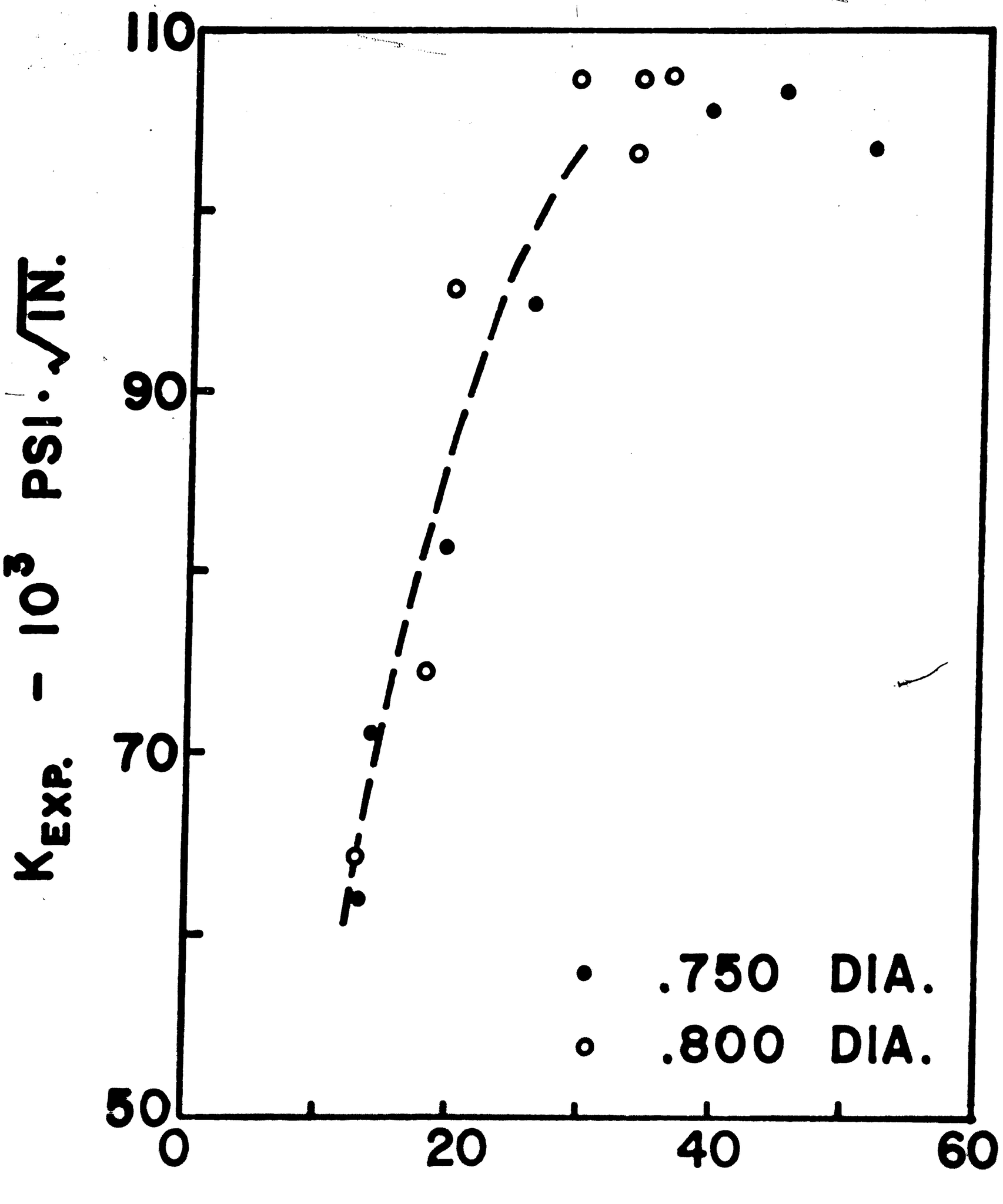

FIG. 11 — $K_{EXP.}$ VS. % SHEAR
- UNPRESSURIZED SPECIMENS.

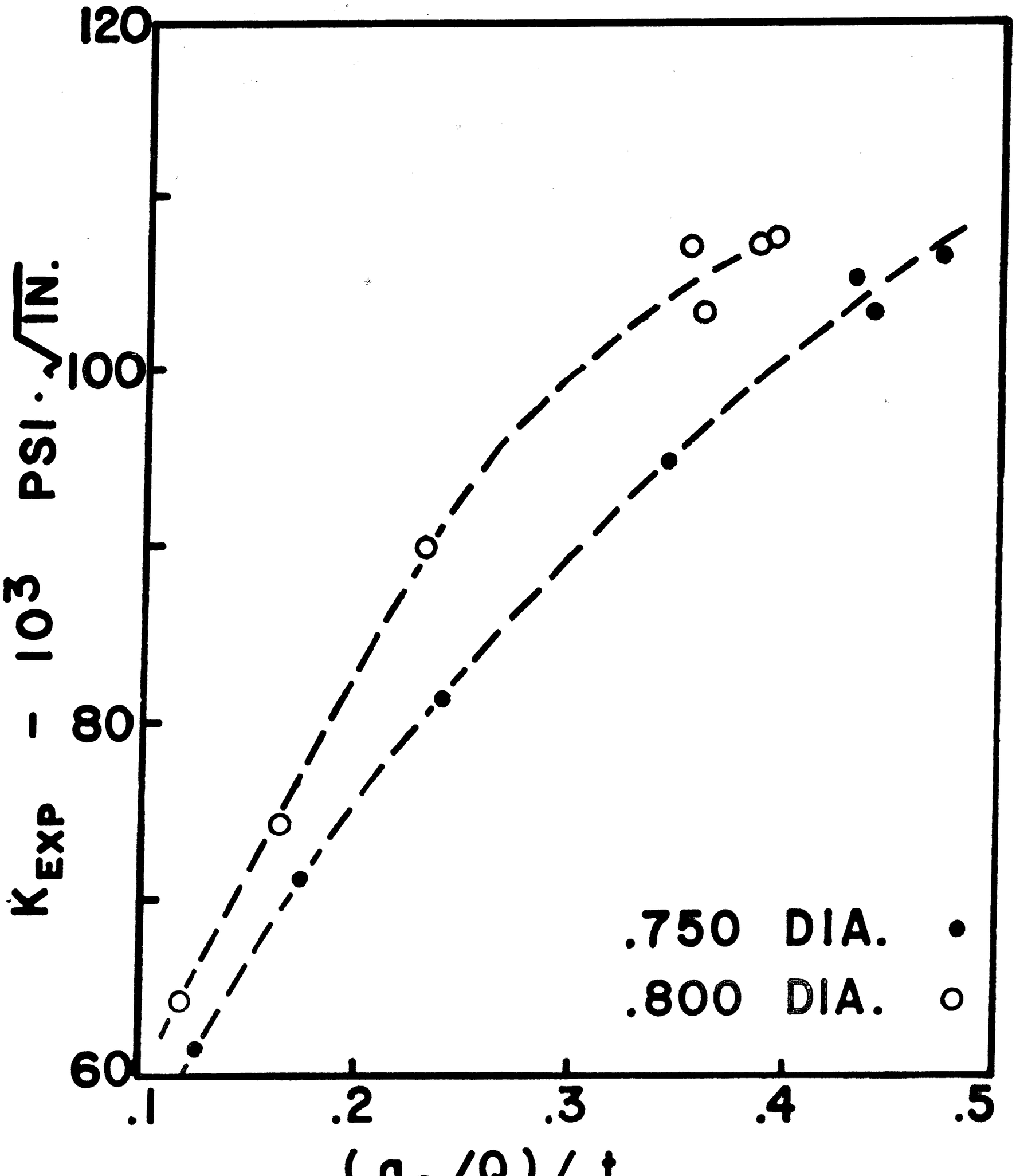

FIG. 12 - K_{EXP} VS. $(a_c/Q)/t$
UNPRESSURIZED SPECIMENS.

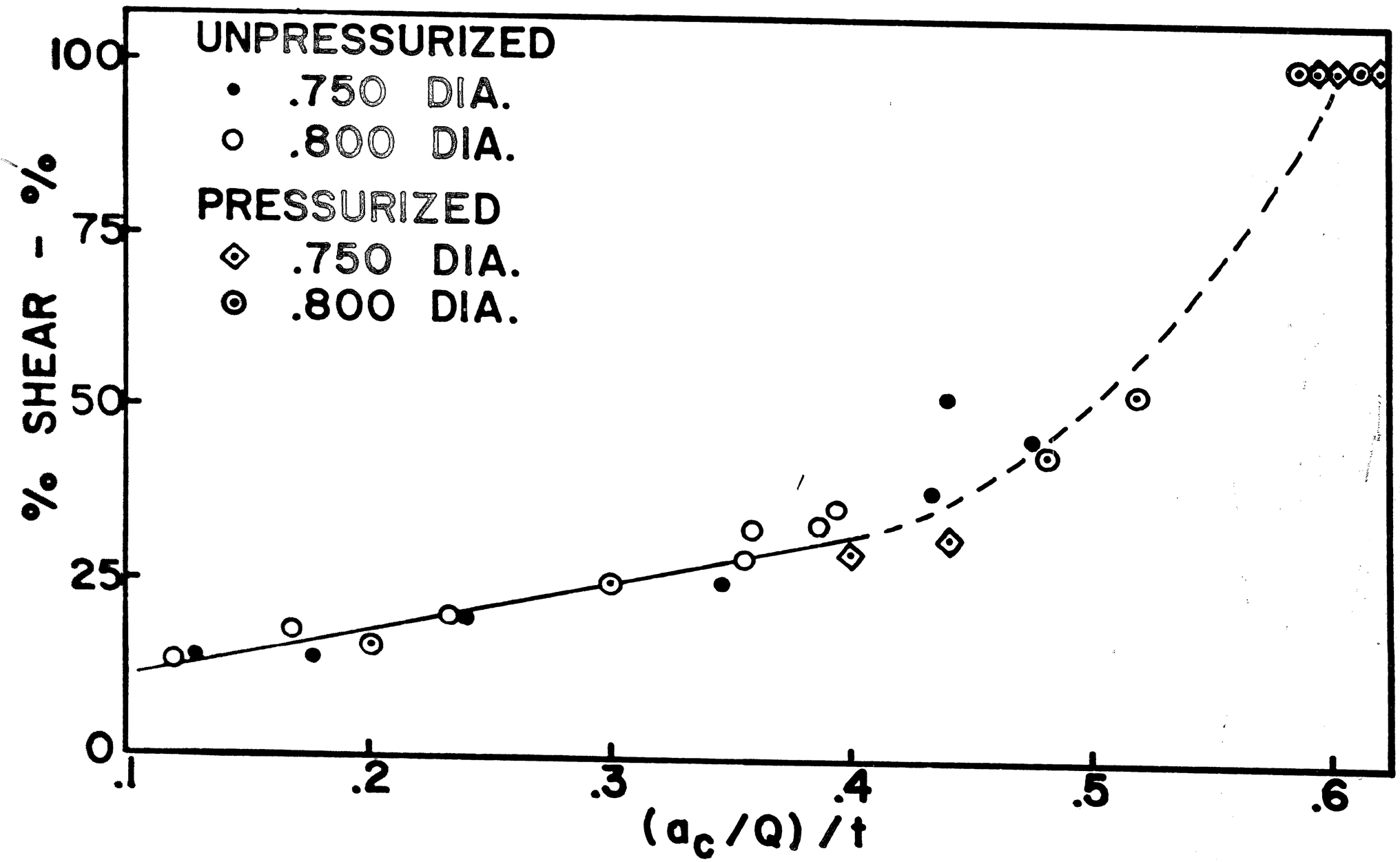

FIG. 13 - % SHEAR VS. $(a_c/Q)/t$.

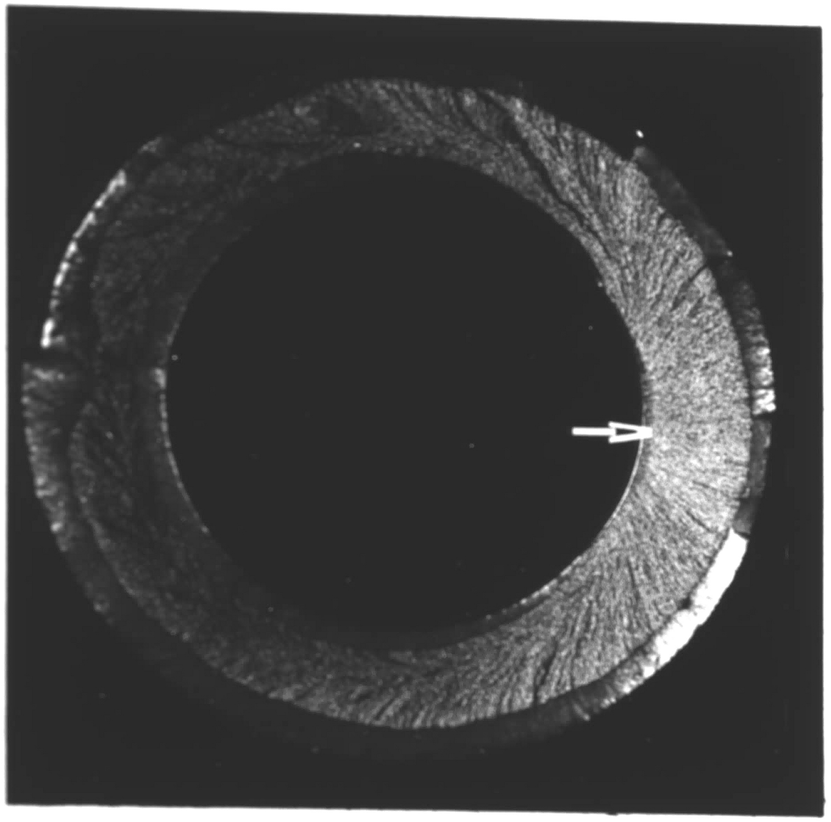

#22
(a = .019 IN.)
4X

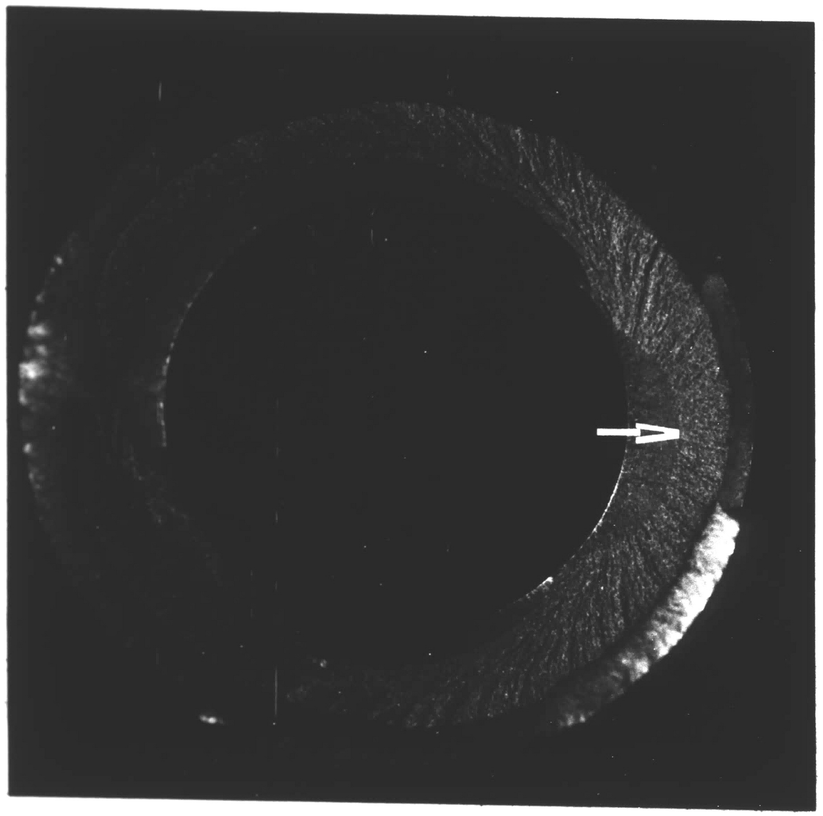

#27
(a = .060 IN.)
4X

FIG. 14 – CRACK DEPTH EFFECT ON SHEAR LIPS – UNPRESSURIZED, .800 IN. DIA. SPECIMENS.

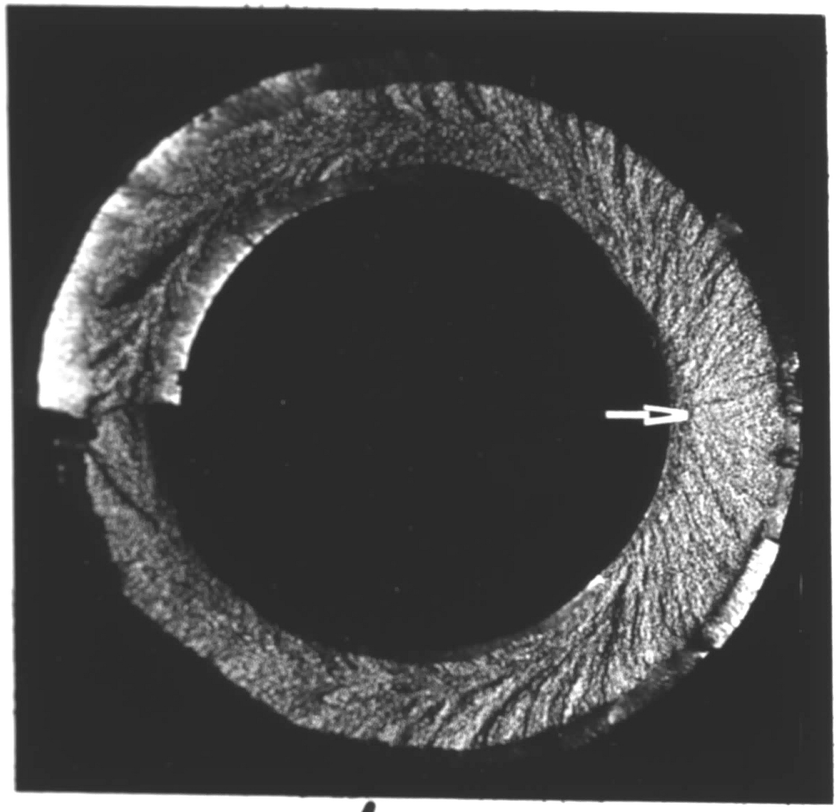

#28P
(a = .021 IN.)
4X

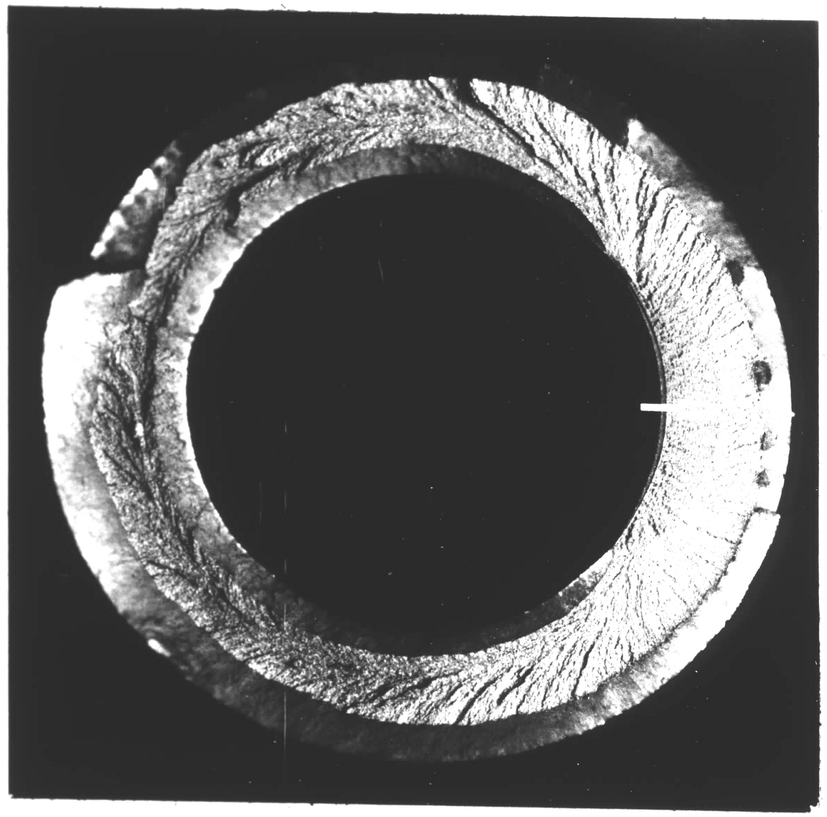

#30P
(a = .061 IN.)
4X

FIG. 15 – CRACK DEPTH EFFECT ON SHEAR LIPS - PRESSURIZED, .800 IN. DIA. SPECIMENS.

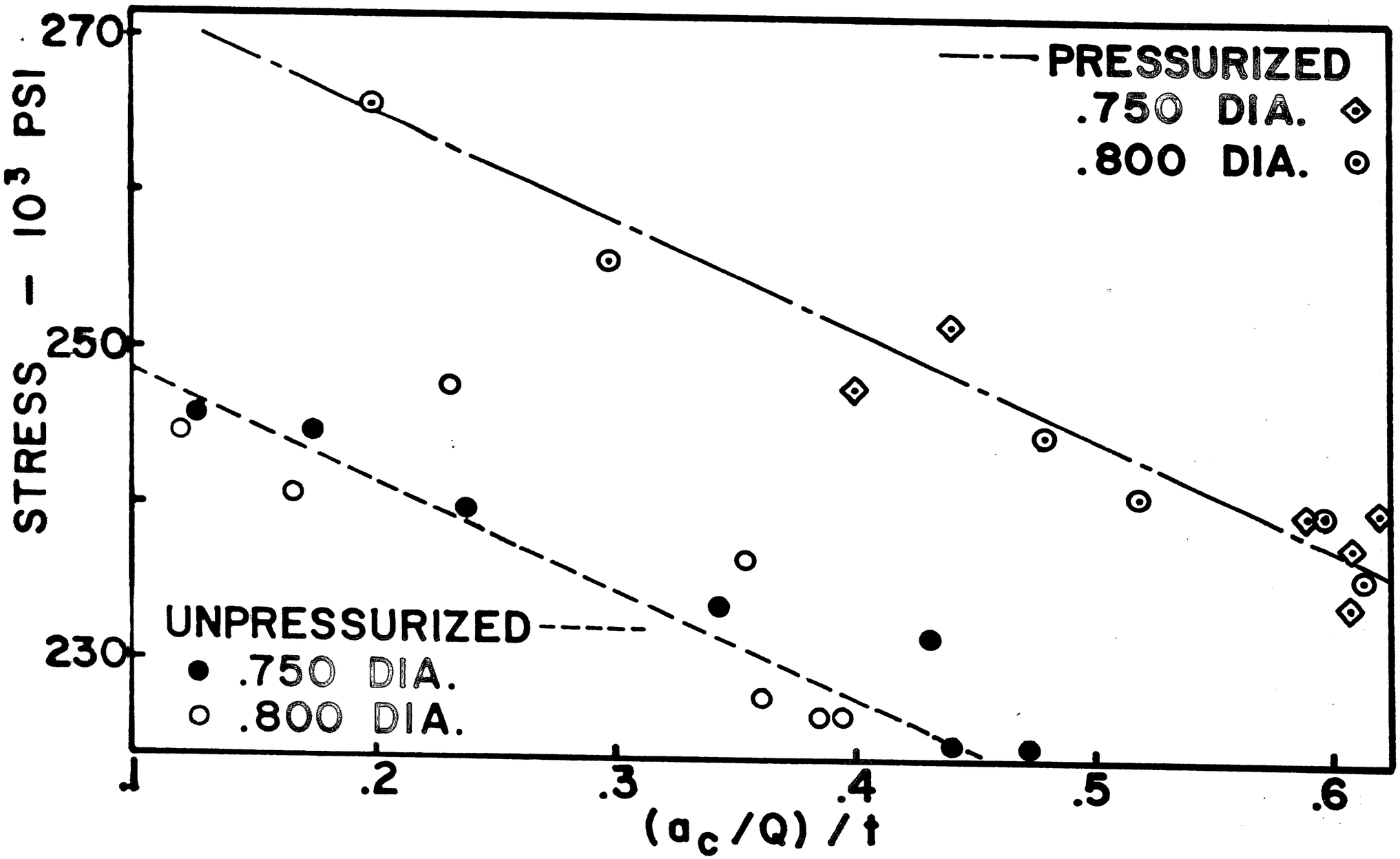

FIG. 16 - VON MISE FRACTURE STRESS VS. $(a_c/Q)/t$.

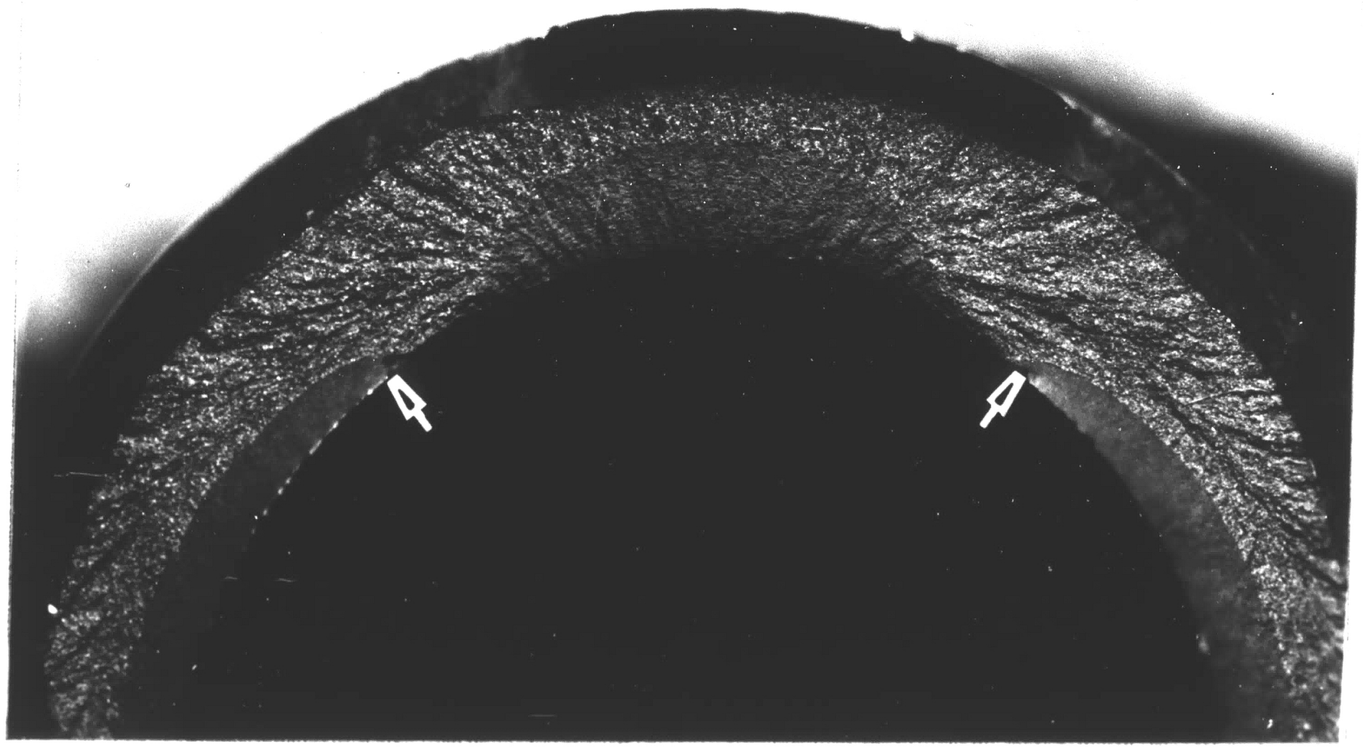

7X

7 - .058 FLAW DEPTH
UNPRESSURIZED

7X

10P - .058 FLAW DEPTH
PRESSURIZED

FIG. 17 - PRESSURE INFLUENCE ON CRITICAL FLAW SHAPE - .750 IN. DIA. SPECIMENS.

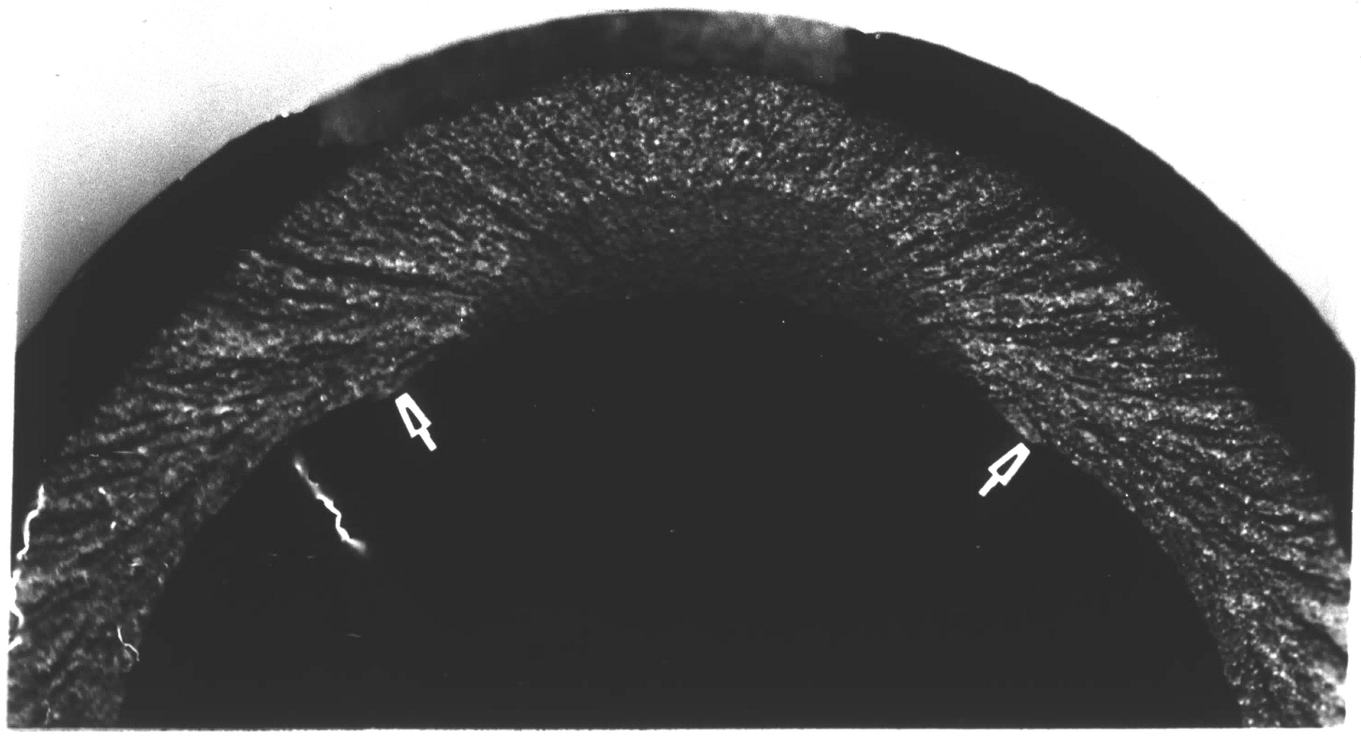

7X

27 - .058 FLAW DEPTH
UNPRESSURIZED

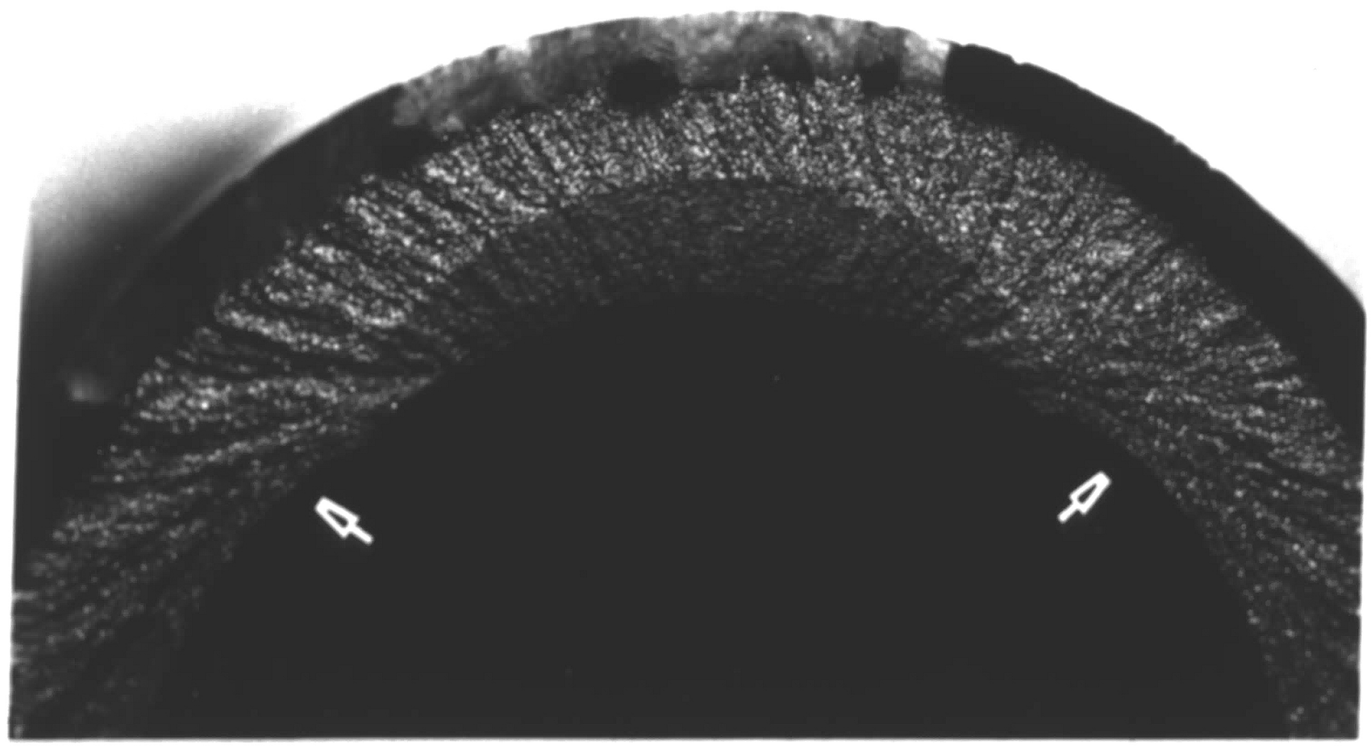

7X

30P - .061 FLAW DEPTH
PRESSURIZED

FIG. 18 - PRESSURE INFLUENCE ON CRITICAL FLAW SHAPE - .800 IN. DIA. SPECIMENS.

TABLE 1 - EXPERIMENTAL TEST DATA FOR .750 DIAMETER SPECIMENS

SPEC-IMEN#	OUTER DIA. (in.)	INNER DIA. (in.)	HARD-NESS R"C"	# FATIGUE CYCLES	LOAD CELL FORCE (lbs.)	SPECIMEN INTERNAL PRESSURE (psi)	EDM DEPTH (in.)	CRITICAL FLAW TOTAL DEPTH (in.)	CRITICAL FLAW CHORD ANGLE (deg.)	FLAT FRACTURE WIDTH (in.)	DUCTILE FRACTURE WIDTH (in.)
1	0.752	0.501	48.5	12500	60700	0	0.0072	0.012	74.6	0.096	0.015
2	0.750	0.502	48.0	51000	59800	0	0.0072	0.016	76.6	0.091	0.015
3	0.750	0.503	47.7	20000	58400	0	0.0067	0.023	72.0	0.078	0.019
4	0.751	0.500	47.2	+7000	57700	0	0.0079	0.036	71.4	0.063	0.022
5	0.751	0.500	46.0	+12000	57200	0	0.0078	0.049	74.6	0.044	0.028
6	0.751	0.500	46.0	+20000	55500	0	0.0065	0.053	73.2	0.032	0.034
7	0.751	0.500	47.1	20000	55600	0	0.0068	0.058	76.4	0.033	0.029
8P	0.750	0.501	49.3	51000	52600	53400	0.0073	0.041	83.4	0.054	0.023
9P	0.750	0.500	48.0	20000	52500	60000	0.0073	0.046	76.6	0.049	0.023
10P	0.751	0.500	48.7	20000	50400	61000	0.0068	0.058	132.6	0.000	0.057
11P	0.750	0.500	47.0	20000	48700	66200	0.0079	0.060	132.0	0.000	0.056
12P	0.751	0.500	48.1	10000	51100	58300	0.0077	0.061	120.5	0.000	0.056
13P	0.750	0.501	48.0	20000	49200	59800	0.0073	0.063	130.4	0.000	0.053

TABLE 2 - EXPERIMENTAL TEST DATA FOR .800 DIAMETER SPECIMENS

SPECIMEN#	OUTER DIA. (in.)	INNER DIA. (in.)	HARDNESS R"C"	# FATIGUE CYCLES	LOAD CELL FORCE (lbs.)	SPECIMEN INTERNAL PRESSURE (psi)	EDM DEPTH (in.)	CRITICAL FLAW TOTAL DEPTH (in.)	CRITICAL FLAW CHORD ANGLE (deg.)	FLAT FRACTURE WIDTH (in.)	DUCTILE FRACTURE WIDTH (in.)
21	0.802	0.505	47.9	12000	74800	0	0.0062	0.013	68.2	0.114	0.017
22	0.802	0.505	48.3	19000	73600	0	0.0064	0.019	68.6	0.103	0.023
23	0.801	0.500	47.8	54000	76200	0	0.0068	0.027	71.4	0.097	0.024
24	0.800	0.500	46.1	15000	72600	0	0.0062	0.048	71.4	0.068	0.028
25	0.801	0.500	46.2	+19000	70200	0	0.0064	0.051	70.2	0.062	0.031
26	0.802	0.500	46.6	+16000	70200	0	0.0067	0.059	73.4	0.055	0.031
27	0.802	0.500	47.4	20000	70200	0	0.0069	0.060	74.0	0.055	0.028
28P	0.801	0.501	48.4	19000	68500	59900	0.0070	0.021	80.0	0.105	0.020
29P	0.801	0.500	49.3	19000	67800	59800	0.0072	0.036	79.8	0.086	0.028
30P	0.801	0.500	47.9	19000	67800	58800	0.0064	0.061	100.4	0.044	0.035
31P	0.801	0.500	48.8	10000	66500	60200	0.0074	0.068	109.4	0.035	0.039
32P	0.800	0.500	47.6	19000	63000	67600	0.0066	0.071	169.6	0.000	0.068
33P	0.801	0.500	48.2	10000	66400	60600	0.0065	0.071	146.6	0.000	0.071

TABLE 3 - CALCULATIONS FOR UNPRESSURIZED SPECIMENS

SPECIMEN #	K_{exp} (ksi $\sqrt{in.}$)	AXIAL GROSS STRESS (ksi)	AXIAL NET STRESS (ksi)	YIELD STRENGTH (ksi)	a/2c	Φ^2	(a_c/Q) (in.)	PERCENT SHEAR (%)	VON MISES FRACTURE STRESS (ksi)
1	62.1	246	249	205	0.036	1.019	0.016	13.5	246
2	71.3	245	250	203	0.047	1.029	0.022	14.1	245
3	81.7	240	246	200	0.073	1.063	0.030	19.5	240
4	95.0	234	243	197	0.115	1.129	0.043	25.8	234
5	105.9	232	244	192	0.150	1.204	0.054	38.8	232
6	103.7	225	238	192	0.166	1.241	0.055	51.5	225
7	106.8	226	240	197	0.174	1.259	0.059	46.7	226
21	64.5	245	248	203	0.043	1.026	0.018	12.9	245
22	74.6	242	245	205	0.063	1.051	0.025	18.2	242
23	90.6	248	253	203	0.086	1.084	0.035	19.8	248
24	107.4	237	247	192	0.154	1.213	0.053	29.1	237
25	103.5	228	238	192	0.166	1.243	0.054	33.3	228
26	107.8	227	239	195	0.184	1.286	0.059	36.0	227
27	107.6	227	239	200	0.185	1.292	0.058	33.7	227

TABLE 4 - CALCULATIONS FOR PRESSURIZED SPECIMENS

SPECIMEN #	K_{exp} (ksi $\sqrt{in.}$)	AXIAL GROSS STRESS (ksi)	AXIAL NET STRESS (ksi)	YIELD STRENGTH (ksi)	a/2c	Φ^2	(a_c/Q) (in.)	PERCENT SHEAR (%)	VON MISES FRACTURE STRESS (ksi)
8P	112.7	258	271	211	0.112	1.133	0.050	29.8	248
9P	120.5	262	276	203	0.137	1.180	0.055	31.9	252
10P	134.2	253	283	205	0.100	1.106	0.074	100.0	240
11P	137.2	252	283	197	0.104	1.112	0.078	100.0	240
12P	136.4	254	283	203	0.116	1.133	0.076	100.0	238
13P	134.6	249	282	208	0.110	1.125	0.076	100.0	234
28P	88.4	262	267	205	0.060	1.045	0.030	16.0	266
29P	107.4	259	267	211	0.103	1.113	0.045	24.5	256
30P	135.8	258	277	203	0.139	1.180	0.072	44.3	245
31P	138.8	255	278	208	0.142	1.189	0.078	52.7	241
32P	147.6	249	288	200	0.096	1.097	0.092	100.0	236
33P	148.7	255	288	203	0.111	1.125	0.089	100.0	240

REFERENCES

1. Weiss, V., "Current Views and Theories on Fracture, Crack Initiation and Propagation, "Proceedings, Seventh Sagamore Ordinance Materials Research Conference, Syracuse University, Syracuse, New York, 1960.

2. Irwin, G. R., "Relation of Crack Toughness Measurements to Practical Applications, "Welding Journal Research Supplement, Vol. 41 (1962), p. 519S.

3. ASTM Special Committee on Fracture Testing of High-Strength Metallic Materials, "Progress in the Measurement of Fracture Toughness and the Application of Fracture Mechanics to Engineering Problems, "Materials Research & Standards, Vol. 4 (1964), p. 107.

4. Paris, P. C., and G. C. Sih, "Stress Analysis of Cracks," Fracture Toughness Testing and Its Applications, ASTM STP 381, Am. Soc. Testing Materials, Phil., 1965, p. 30.

5. Osgood, C. S., "Applying Fracture Mechanics to Design," Machine Design, Vol. 85 (1963), p. 102.

6. Ang, D. D., E. S. Folias, and M. L. Williams, "The Bending Stress in a Cracked Plate on an Elastic Foundation," Journal of Applied Mechanics, Vol. 85 (1963), p. 245.

7. Sih, G., and D. Setzer, published discussion of "The Bending Stress in a Cracked Plate on an Elastic Foundation," Journal of Applied Mechanics, Vol. 86 (1964), p. 365.

8. Tiffany, C. F., P. M. Lorenz, and L. R. Hall, "Investigation of Plane-Strain Flaw Growth in Thick-Walled Tanks," NASA CR-54837, National Aeronautics and Space Administration, The Boeing Co., Seattle, Wash., February, 1966.

9. Kibler, J. J., and R. Roberts, "The Effect of Biaxial Stresses on Fatigue and Fracture," Journal of Engineering for Industry, Vol. 92 (1970), p. 727.

10. Drucker, D. C., and J. R. Rice, "Plastic Deformation in Brittle and Ductile Fracture," Engineering Fracture Mechanics, Vol. 1 (1970), p. 577.

REFERENCES (cont)

11. Srawley, J. E., and W. F. Brown, Jr., "Fracture Toughness Testing Methods," Fracture Toughness Testing and Its Applications, ASTM STP 381, Am. Soc. Testing Materials, Phil., 1965, p. 133.

12. Irwin, G. R., "Analysis of Stresses and Strains Near the End of a Crack Traversing a Plate," Journal of Applied Mechanics, Vol. 24 (1957), p. 361.

13. Irwin, G. R., "Crack-Extension Force for a Part-Through Crack in a Plate," Journal of Applied Mechanics, Vol. 84 (1962), p. 651.

14. Green, A. E., and I. N. Sneddon, "The Distribution of Stress in the Neighborhood of a Flat Elliptical Crack in an Elastic Solid," Proc. Cambridge Phil. Soc., Vol. 46 (1959).

15. Randall, P. N., "Severity of Natural Flaws as Fracture Origins, and a Study of the Surface-Cracked Specimen," AFML-TR-66-204, Air Force Material Lab., Dayton, Ohio, August, 1966.

16. Tiffany, C. F., and J. N. Masters, "Applied Fracture Mechanics," Fracture Toughness Testing and Its Applications, ASTM STP 381, Am. Soc. Testing Materials, Phil., 1965, p. 249.

17. "Tentative Method of Test for Plane Strain Fracture Toughness of Metallic Materials," E-399-70 T, ASTM Committee E-24 on Fracture Testing of Metals, March, 1970.

18. Amateau, M. F., and E. A. Steigerwald, "Fracture Characteristics of Structural Metals," AD 611873, ER-5937-3, Thompson-Ramo-Wooldridge, Cleveland, Ohio, January, 1965.

19. Wessel, E. T., W. G. Clark, and W. K. Wilson, "Engineering Methods for the Design and Selection of Materials Against Fracture," OMS 5025.11.26800.01.01, Ordinance Management Structure, Westinghouse Research Laboratories, Pittsburgh, Pa., June, 1966.

20. Brown, W. F., Jr., and J. E. Srawley, Plane Strain Crack Toughness Testing of High Strength Metallic Materials, ASTM STP 410, Am. Soc. Testing Materials, Phil., 1965.

21. Personal Communication, Vanadium-Alloys Steel Company, Latrobe, Pa.

REFERENCES (cont)

22. Irwin, G. R., "Fracture Mode Transition for a Crack Traversing a Plate," Journal of Basic Engineering, Vol. 82 (1960), p. 417.

23. Dieter, G. E., Jr., Mechanical Metallurgy, McGraw-Hill Book Co., New York, 1961.

24. Spotts, M. F., Mechanical Design Analysis, Englewood Cliffs, N. J.: Prentice-Hall, Inc., 1964.

25. Johnson, H. H., and P. C. Paris, "Sub-Critical Flaw Growth," Engineering Fracture Mechanics, Vol. 1 (1968), p. 3.

26. Hartranft, R. J., and G. C. Sih, "Alternating Method Applied to Edge and Surface Crack Problems," NASA-TR-72-1, National Aeronautics and Space Administration, Lehigh University, Bethlehem, Pa., April, 1972.

VITA

Ralph N. Binkley was born on December 25, 1933, in Utica, Michigan. He attended elementary school and high school in Hazel Park, Michigan. After graduation in 1951, he worked for several years and served time in the USAF.

He graduated from Indiana Institute of Technology in 1961 with a B. S. in Mechanical Engineering. The next seven years he worked for Delco Remy Division, G.M.C. in manufacturing engineering. During this time, he obtained his Professional Engineer's License in Indiana.

In 1968 he joined the Western Electric Company at Indianapolis, Indiana, and in 1970 he entered the Graduate School of Lehigh University as a member of Western Electric Lehigh Master's Program.